Backward-Facing Step Flows for Various Expansion Ratios at Low and Moderate Reynolds Numbers

G. Biswas*

M. Breuer

F. Durst

Lehrstuhl für Strömungsmechanik,
Universität Erlangen-Nürnberg Cauerstr. 4,
D-91058 Erlangen, Germany
e-mail: breuer@lstm.uni-erlangen.de

This paper is concerned with the behavior of flows over a backward-facing step geometry for various expansion ratios $H/h=1.9423$, 2.5 and 3.0. A literature survey was carried out and it was found that the flow shows a strong two-dimensional behavior, on the plane of symmetry, for Reynolds numbers $Re_D=\rho U_b D/\mu$ below approximately 400 (U_b =bulk velocity and D=hydraulic diameter). In this Reynolds number range, two-dimensional predictions were carried out to provide information on the general integral properties of backward-facing step flows, on mean velocity distributions and streamlines. Information on characteristic flow patterns is provided for a wide Reynolds number range, $10^{-4}\leqslant Re_D\leqslant 800$. In the limiting case of $Re_D\rightarrow 0$, a sequence of Moffatt eddies of decreasing size and intensity is verified to exist in the concave corner also at $Re_D=1$. The irreversible pressure losses are determined for various Reynolds numbers as a function of the expansion ratio. The two-dimensional simulations are known to underpredict the primary reattachment length for Reynolds numbers beyond which the actual flow is observed to be three-dimensional. The spatial evolution of jet-like flows in both the streamwise and the spanwise direction and transition to three-dimensionality were studied at a Reynolds number $Re_D=648$. This three-dimensional analysis with the same geometry and flow conditions as reported by Armaly et al. (1983) reveals the formation of wall jets at the side wall within the separating shear layer. The wall jets formed by the spanwise component of the velocity move towards the symmetry plane of the channel. A self-similar wall-jet profile emerges at different spanwise locations starting with the vicinity of the side wall. These results complement information on backward-facing step flows that is available in the literature. [DOI: 10.1115/1.1760532]

1 Introduction and Aim of Work

This paper is concerned with two- and three-dimensional backward-facing step flows and provides results obtained by thorough numerical computations for various expansion ratios and a wide Reynolds number range. Although numerous investigations have been carried out on this topic, an insightful and complete understanding of the physical origin of flow separation and vortex formation has hitherto been not clear. The major reason for this lies in the fact that an analytical treatment of the flow is not available and hence experimental and numerical investigations are involved. Most studies on backward-facing step flows were carried out for a limited number of relevant parameters such as Reynolds number $\mathrm{Re}_D=\rho U_b D/\mu$, expansion ratio H/h and aspect ratio W/h. Here $D=2h$ denotes the hydraulic diameter of the inlet channel with height h, H the channel height in the expanded region and W the channel width. Other definitions of the Reynolds numbers found in the literature will be provided in Section 3.1. Because of this situation, distributed results are available in various publications. Furthermore, the existing investigations are partially incomplete with respect to the relevant parameter sets and require extensions to provide the basis for a sufficiently detailed fluid mechanical knowledge of backward-facing step flows. This paper is a contribution to improve the present unsatisfactory situation, at least for the Reynolds number range $10^{-4}\leqslant \mathrm{Re}_D\leqslant 800$ and the expansion ratio range $1.9423\leqslant H/h\leqslant 3$. The flow obeys the laws of two-dimensionality on the vertical mid-plane, i.e. on the plane which is equidistant from the two side walls, up to a Reynolds number of 400. For this range of Reynolds numbers, a fairly complete description of the flow is provided. Attempts have been made to explain the mechanisms that are responsible for the difference in the prediction of primary recirculation length for two- and three-dimensional simulations.

The backward-facing step flow was already of interest even when fluid mechanical problems used to be addressed only by potential flow theory. As shown by Lee and Smith [1], potential flow theory permits the treatment of the backward-facing step flow yielding a streamline pattern which does not indicate any separation or recirculation region behind the step. Hence potential theory does not provide the generally expected separation of the flow at the upper corner of the step, nor does the lower corner yield a region of vortices as expected from the considerations of Moffatt [2]. Moffatt predicted under specified conditions the existence of a sequence of vortices near corners as shown in Fig. 1 for $\mathrm{Re}_D\rightarrow 0$. Early numerical predictions of backward-facing step flows, see, e.g., Roache [3], Taylor and Ndefo [4] and Durst and Pereira [5], did not show any separation at the upper corner of the step for low Reynolds numbers. However, a separated region was predicted at the lower corner that contained a single vortex only. A careful analysis of the flow in sudden expansions was carried out by Alleborn et al. [6] and it was indicated that, at least at low Reynolds numbers, the lower corner contains a sequence of Moffatt vortices. It was concluded by Alleborn et al. [6] that the earlier numerical predictions were carried out with insufficient numerical grid resolution to resolve the smaller vortices at the lower corner. Hence high-performance computers are needed to carry out detailed studies of backward-facing step flows, even at low Reynolds numbers. Furthermore, since the early work to predict the backward-facing step flows, new numerical methodologies such as the multigrid method (see, e.g., Brandt et al. [7], Hackbusch [8]) or local block refinement (see, e.g., Lange et al. [9]) have been introduced into computer programs for solving the

*Present address: Mechanical Engineering Department, Indian Institute of Technology, Kanpur-208016, India.

Contributed by the Fluids Engineering Division for publication in the JOURNAL OF FLUIDS ENGINEERING. Manuscript received by the Fluids Engineering Division March 6, 2003; revised manuscript received November 8, 2003. Associate Editor: F. F. Grinstein.

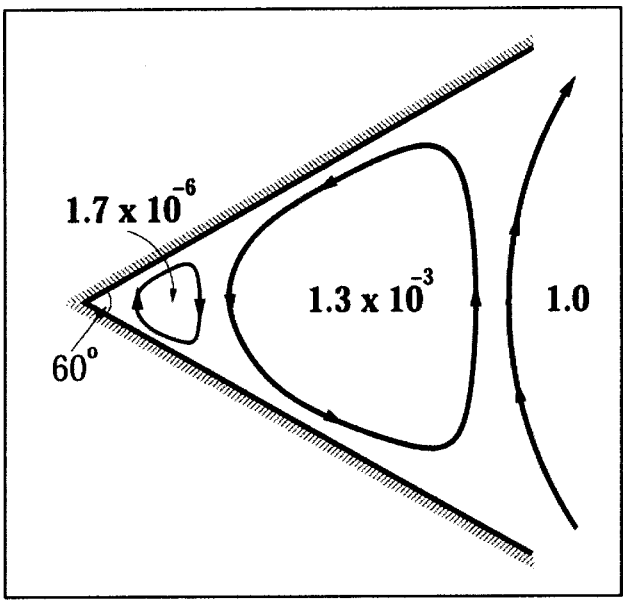

Fig. 1 Moffatt eddies in a concave corner for $2\alpha=60$ deg. The values describe the relative intensities (Moffatt [2]).

Navier-Stokes equations more efficiently with a faster convergence rate. It is also claimed that most of the numerical predictions on backward-facing step flows that have been carried out have not resolved the corner singularity at the step and its effect on the velocity field, see Ladevéze and Peyret [10].

Furthermore, the mechanisms that are responsible for increasing primary reattachment length resulting from the two-dimensional to three-dimensional flow transition are not completely understood. One possible reason for the difference in two- and three-dimensional predictions could be the effects initiated at the side walls of the channel, see Armaly et al. [11]. Durst et al. [12] have observed a symmetry-breaking bifurcation leading to one short and one long primary separation zone in a sudden-expansion flow.

This paper provides a brief literature survey carried out to summarize the existing knowledge on backward-facing step flows under the conditions mentioned above. The basic equations and their numerical solution methods, including the boundary conditions employed, are summarized in Section 3. In Section 4 the results are provided and the paper is concluded in Section 5.

2 Backward-Facing Step Flow: A Brief Literature Survey

The study of backward-facing step flows constitutes an important branch of fundamental fluid mechanics. The interest in such a flow was intensified with the experimental and numerical work of Armaly et al. [11]. They presented a detailed experimental investigation in a backward-facing step geometry for an expansion ratio $H/h=1.9423$, an aspect ratio $W/h=35$ and Reynolds numbers up to $\mathrm{Re}_D=8000$. The flow appeared to be three-dimensional above Reynolds numbers close to 400. Around this Reynolds number, they observed a discrepancy in the primary recirculation length between the experimental results and the numerical predictions. Also, around this Reynolds number, a secondary recirculation zone was observed at the channel upper wall. Armaly et al. [11] conjectured that the discrepancy between the experimental measurements and the numerical prediction was due to the secondary recirculation zone that perturbed the two-dimensional character of the flow. The normalized value of the reattachment length showed a peak at $\mathrm{Re}_D\approx1{,}200$. The decrease in recirculation length beyond a Reynolds number of 1,200 was attributed to the effect of Reynolds stresses.

Kim and Moin [13] computed the flow over a backward-facing step using a method that is second-order accurate in both space and time. They found a dependence of the reattachment length on Reynolds number in good agreement with the experimental data of Armaly et al. [11] up to about $\mathrm{Re}_D=500$. At $\mathrm{Re}_D=600$ the computed results of Kim and Moin [13] started to deviate from the experimental values. The difference was attributed to the three-dimensionality of the experimental flow around a Reynolds number of 600.

Gartling [14] developed a solution procedure using a Galerkin-based finite-element method for steady incompressible flow over a backward-facing step geometry. His results compared well, especially with respect to the bottom wall separation zone, with the results of Kim and Moin [13].

Lee and Mateescu [15] performed an experimental and numerical investigation of air flow over a two-dimensional backward-facing step for $\mathrm{Re}_D\leqslant3000$. The hot film sensor measurements at $\mathrm{Re}_D=805$ and expansion ratio $H/h=2.0$ were found to be in agreement with their numerical predictions with respect to the locations of the separation and reattachment points on the upper and lower walls.

Kaiktsis et al. [16] identified the bifurcation of two-dimensional laminar flow to three-dimensional flow as the primary source of discrepancies appearing in comparisons of numerical predictions and experimental data. They also observed that irrespective of the accuracy of the numerical schemes, the experimentally measured recirculation lengths (Armaly et al. [11]) were consistently underestimated above a Reynolds number of $\mathrm{Re}_D=600$. They found that all unsteady states of the flow are three-dimensional and develop for Reynolds number $\mathrm{Re}_D\geqslant\mathrm{Re}_c\approx700$. Furthermore, they detected that the downstream flow region is excited through the upstream shear layer with a characteristic frequency f_1. The supercritical states ($\mathrm{Re}_D>700$) were found to be periodic with another incommensurate frequency, f_2.

Durst et al. [12] observed the formation of secondary separation zones in the two-dimensional numerical simulations of a symmetric sudden-expansion flow. This observation is similar to what is found in the backward-facing step flow. Both the experiments and the predictions confirm a symmetry-breaking bifurcation leading to one short and one long primary separation zone.

Kaiktsis et al. [17] revisited the backward-facing step flow and found that the unsteadiness in step flow was created by convective instabilities. Another important conclusion of this study is that the upstream-generated small disturbances propagate downstream at exponentially amplified amplitude with a space-dependent speed in the range $700\leqslant\mathrm{Re}_D\leqslant2500$.

Heenan and Morrison [18] conducted experiments for a Reynolds number (Re_S) based on the step height S of 1.9×10^5 and suggested that while the flow is likely to be convectively unstable over a large region, the global unsteadiness, driven by the impingement of large eddies at reattachment is the cause of low frequency oscillations called *flapping*.

Le et al. [19] conducted direct numerical simulations of turbulent flows over a backward-facing step at a Reynolds number of $\mathrm{Re}_S=5100$ based on step height S and inlet free-stream velocity, and an expansion ratio of 1.2. The instantaneous velocity fields reveal the variation of reattachment length in the spanwise direction that oscillates about a mean value of 6.28 S. The flow exhibits strong streamwise vortical structures.

Kaltenbach and Janke [20] investigated the effect of sweep on the transitional separation bubble behind a backward-facing step using direct numerical simulation. In this context they also performed simulations for the unswept case at $\mathrm{Re}_S=3000$. The flow upstream of the step was laminar and shear-layer transition took place prior to reattachment. Comparing the results for zero sweep from two simulations using either steady inflow conditions or the same velocity profiles with superimposed low-amplitude random disturbances, they found out that the flow field downstream of the step is very sensitive to the type of inlet boundary conditions. The

changes in global flow features which are due to sweep, seem to be fairly independent of the specific transition scenario.

Williams and Baker [21] investigated laminar flow over a three-dimensional backward-facing step geometry. The full three-dimensional simulation of the geometry of Armaly et al. [11] for $100 \leqslant \mathrm{Re}_D \leqslant 800$ correctly predicts the reattachment lengths and confirms the effect of three-dimensionality. They also found that the side walls result in the creation of a wall jet, located at the lower channel wall and pointing from the side wall towards the channel mid-plane.

Chiang and Sheu [22] performed three-dimensional simulations of the laminar flow in a step geometry with an expansion ratio similar to that of Armaly et al. [11] for various Reynolds numbers and aspect ratios. They found that the flow at the plane of symmetry develops into a two-dimensional like profile only if the aspect ratios are increased up to 50 and higher.

Recently, Barkley et al. [23] carried out a three-dimensional linear stability analysis for the backward-facing step flow with an expansion ratio of 2. They showed that the primary bifurcation of the steady, two-dimensional flow is a steady, three-dimensional instability. Furthermore, the critical eigenmode is localized to the primary recirculation region consisting of a flat roll.

Nie and Armaly [24] presented the results of laminar forced convection flow in a backward-facing step geometry. They showed that the size of the primary recirculation zone and the maximum Nusselt number increase with increasing step height. They also indicated that the jet-like flow that develops near the side wall impinges on the stepped wall, causing a minimum to develop in the reattachment length near the side wall.

3 Numerical Methodology

3.1 Governing Equations. An incompressible fluid with constant fluid properties is assumed. The dimensionless governing equations expressing the conservation of mass and momentum are, in Cartesian coordinates x_j, as follows:

$$\frac{\partial u_j}{\partial x_j} = 0, \tag{1}$$

$$\frac{\partial u_i}{\partial t} + \frac{\partial (u_i u_j)}{\partial x_j} = -\frac{\partial p}{\partial x_i} - \frac{1}{\mathrm{Re}} \frac{\partial \tau_{ij}^{mol}}{\partial x_j} \tag{2}$$

where $i,j = 1-3$. The Cartesian velocity components are denoted u_j and the pressure p. τ_{ij}^{mol} describes the molecular momentum transport, which for a Newtonian fluid can be expressed by

$$\tau_{ij}^{mol} = -\mu \left(\frac{\partial u_i}{\partial x_j} + \frac{\partial u_j}{\partial x_i} \right). \tag{3}$$

The only non-dimensional parameter appearing in the governing equations is the Reynolds number. For the flow problem considered, the following definition is used:

$$\mathrm{Re} = \mathrm{Re}_D = \frac{\rho U_b D}{\mu}, \tag{4}$$

where ρ and μ are the density and the dynamic viscosity, respectively. As mentioned before, U_b denotes the bulk (average) velocity of the inlet flow, which corresponds in the laminar case to two-thirds of the maximum inlet velocity. In the present investigation the notation of Armaly et al. [11] is used, where D is chosen as the hydraulic diameter of the inlet channel, which is equivalent to twice its height, $D = 2h$. For the definition of the characteristic length, different options are used in the literature leading to the following additional definitions of the Reynolds number:

$$\mathrm{Re}_h = \frac{\rho U_b h}{\mu},$$

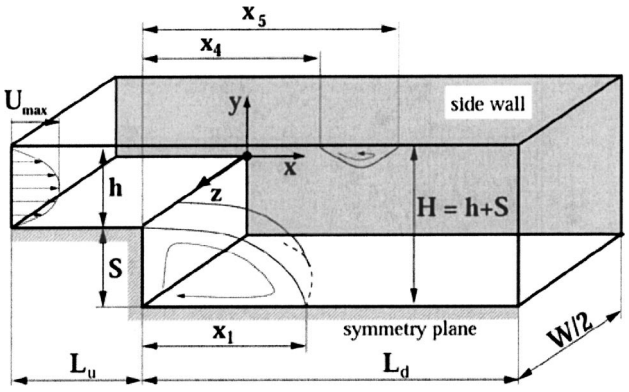

Fig. 2 Sketch of the flow configuration and definition of length scales

$$\mathrm{Re}_S = \frac{\rho U_b S}{\mu},$$

where h is the channel height upstream of the step and S denotes the step height (see Fig. 2). All three definitions are in use for backward-facing step flows, which requires a clear statement on the definition applied (here: Re_D in order to avoid confusion).

3.2 Geometry of the Flow Domain and Boundary Conditions. The geometry of the flow problem was chosen in accordance to the experimental setup of Armaly et al. [11] sketched in Fig. 2. The expansion ratio is defined by $H/h = 1 + S/h$, i.e., by the ratio of the channel height H downstream of the step to the channel height h of the inflow channel, where S denotes the step height. In addition to Armaly et al.'s expansion ratio of $H/h = 1.9423$, two other configurations with larger step heights S were considered, i.e., $H/h = 2.5$ and 3.0. For the three-dimensional predictions, the aspect ratio W/h was set to 35 and only half of the geometry is taken into account assuming symmetry at $z = W/2$. Furthermore, the two-dimensional computations are restricted to this symmetry plane. The assumption of spanwise symmetry in the three-dimensional computations was carefully checked by additional simulations based on periodic boundary conditions in spanwise direction. The predicted results for the plane of symmetry ($z = W/2$) using both types of boundary conditions were found to deviate negligibly, e.g., the discrepancies with respect to the computed length of the different recirculation regions were found to be about 0.01%.

Upstream and downstream of the step, the channel length is L_u and L_d, respectively. Note that in the present study all geometrical length scales are made dimensionless based on the channel height h. In order to simulate a fully developed laminar channel flow upstream of the step, a standard parabolic velocity profile with a maximum velocity $U_{\max} = 3/2 U_b$ is prescribed at the channel inlet ($x = -L_u$) for the two-dimensional model. For the three-dimensional simulations a curve fit of the experimental data of Armaly et al. [11] was used as the inlet conditions. In the laminar range, the measured profile of Armaly et al. was close to the solution of the fully developed duct flow with a rectangular cross-section (see White [25]) showing a slight deviation from the two-dimensional parabolic profile.

Based on a series of simulations carried out with different upstream lengths L_u showing no influence on the predicted results past the step for $L_u \geqslant 5h$, a distance of five times the channel height h upstream of the step expansion was verified to be absolutely sufficient. This coincides with data reported in the literature. At the outlet of the computational domain ($x = L_d$) the flow should be fully developed again. Hence, the application of simple outflow conditions assuming zero gradients of all flow variables is typically sufficient. However, to be on the safe side, we also tested a convective boundary condition (Orlanski [26]) at the outflow

Table 1 Grid-independence study at $Re_D=100$ $H/h=1.9423$ using five consecutively refined grid levels (finest grid=5, coarsest grid=1)

Grid Level	$\Delta y_{min}/h$	x_1/h	*Error*	*Error* [%]
Richardson extrapolation	–	2.70584	–	–
5	0.01	2.70305	0.0027933	0.103
4	0.02	2.69467	0.0111733	0.413
3	0.04	2.67253	0.0333133	1.231
2	0.08	2.61510	0.0907433	3.353
1	0.16	2.36366	0.3421833	12.646

plane, but that yielded no deviations to the Neumann condition. The convective boundary condition ensures that vortices can approach and pass the outflow boundary without significant disturbances or reflections into the inner domain. This property was justified based on large-eddy simulations (LES) for various flows (see, e.g., Breuer and Rodi [27] or Breuer [28,29]).

In the range of Reynolds numbers investigated, the flow is affected very little by the outflow length L_d assuming that the length of the flow development was correctly estimated before depending on the Reynolds number. As will be shown below, very short outflow length can be chosen for Reynolds numbers below $Re_D=1$, whereas for the highest value investigated L_d has to be increased to $L_d=32h$. Hence in all cases it was assured that on the one hand the upstream influence of the step does not reach the inflow plane and on the other hand that the flow is fully developed at the outlet section. At all solid walls Stokes' no-slip boundary conditions are applied.

3.3 Numerical Solution Method. For the spatial discretization of equations (1)–(3), a finite-volume method (*FASTEST-2D*) with a colocated arrangement of the variables was employed, as described by Demirdžić and Perić [30]. The convection and diffusion terms were evaluated using a central differencing scheme of second-order accuracy. As explained in detail in Breuer [29], a second-order accurate scheme is even appropriate for LES of turbulent flows and consequently is reliable for the simulation of laminar flows carried out within this study. For the pressure calculation, a pressure-correction equation taking mass conservation expressed by equation (1) into account was solved iteratively with equation (2). The entire procedure follows the well-known SIMPLE algorithm (" '*Semi-Implicit Method for Pressure Linked Equation*' ") proposed by Patankar and Spalding [31].

Details of the discretization and the pressure-velocity coupling are given by Demirdžić and Perić [30] and Perić et al. [32]. A nonlinear multigrid scheme was employed for convergence acceleration (see, e.g., Brandt et al. [7] and Hackbusch [8]). For parallel computations, a block-structured grid partitioning and a message-passing strategy were used as described by Durst and Schäfer [33]. In order to improve the accuracy of the numerical results without a decrease in efficiency and to optimize the utilization of the available computational resources, a local grid refinement technique was employed (see Lange et al. [9]). The numerical code *FASTEST-2D* was verified by a variety of predictions for different flow problems, especially for the laminar flow and heat transfer around two-dimensional cylinders at a wide range of Reynolds numbers, see e.g., Lange et al. [34,35], Durst et al. [36] and Shi et al. [37].

In order to investigate whether the predicted results are grid independent, extensive refinement studies were carried out. At least partially, the outcome should be presented here briefly. For that purpose we choose the simulations for expansion ratio $H/h=1.9423$ which were finally based on a grid with about 44,000 control volumes, i.e., the finest grid level (5) of five multigrid levels. In this case the cross-stream direction was resolved by 160 CVs using a wall-normal extension of the first CV of $\Delta y_{min}/h=10^{-2}$. Furthermore, computations on consecutively coarsened grid levels (4, 3, 2, 1) were carried out. As a typical result Table 1 shows the predicted length of the primary recirculation length x_1/h at $Re_D=100$ for all five grid levels. Based on the well-known Richardson extrapolation one can obtain an approximation of the exact solution also provided in Table 1. Using this exact value the absolute and relative errors of the numerical solution on all five grid levels can be determined. It is obvious that the errors monotonically converge towards zero and are only 0.103% on the fifth grid level. If the absolute error is plotted versus the grid spacing (not shown here) with a double-logarithmic scaling of the axes, the slope is as expected for a second-order scheme, at least for the finest grid levels 4 and 5. Additionally, other quantities were taken into account for these extensive refinement studies clearly demonstrating that the results presented in the paper are sufficiently accurate on the finest grid level. These grid-independence studies were repeated at different Reynolds numbers and expansion ratios. For the cases with larger expansion ratios $H/h=2.5$ and 3.0, the total grid resolution has to be increased to about 189,000 and 208,000 CVs, respectively. Further exceptions will be explained in Section 4.

Furthermore, in order to exclude all possibility of doubt, the predictions were partially re-run with a second finite-volume flow solver, *LESOCC*. This code is based on a 3-D finite-volume method for arbitrary non-orthogonal grids (Breuer and Rodi [27], Breuer [28,29]). In accordance with *FASTEST-2D*, all fluxes are approximated by central differences of second-order accuracy. However, time advancement is performed by a predictor-corrector scheme consisting of a low-storage multi-stage Runge-Kutta method (second-order accuracy) for the momentum equations and an implicit solution of the pressure correction equation. Hence the method is especially adapted for three-dimensional unsteady flows, but can also be used for two-dimensional and steady-state predictions. Furthermore, it is highly vectorized and additionally parallelized by domain decomposition allowing efficient computations on high-performance computers.

In the present study, *LESOCC* was used for the three-dimensional cases and the validation purpose mentioned above. For the three-dimensional predictions, a grid consisting of about 4.2 million CVs was employed. Similar to the two-dimensional computations, the wall-normal direction was resolved by 160 CVs, whereas for the spanwise extension 100 CVs were used. Of course, the grid was stretched towards all walls with smallest wall distances of the cell faces of $\Delta y_{min}/h=\Delta z_{min}/h=10^{-2}$. Consequently, a *x-y* cross-section of the grid for the three-dimensional cases was basically identical to the finest grid level of the corresponding grid for the two-dimensional predictions which was verified to be sufficiently fine above.

4 Results of Flow Predictions

For the presentation of the results we first start with the general description of the two-dimensional flow field presented for one expansion ratio and a wide range of Reynolds numbers. Then we address the issues related to various expansion ratios. Subsequently, we discuss in detail the flow fields for the three-dimensional simulations and identify the spatial spanwise structures. In a subsequent section, we attempt to predict some integral parameters of practical interest.

4.1 Two-Dimensional Predictions

4.1.1 Flow Field. Figure 3 shows streamlines of the steady-state flow field for an expansion ratio $H/h=1.9423$ (≈ 2) and a Reynolds number range $10^{-4} \leqslant Re_D \leqslant 10^2$. This expansion ratio was considered in the experimental study by Armaly et al. [11] and the same value has been used for a set of numerical computations. The flow over the backward-facing step is two-dimensional and non-oscillatory in the region of $Re_D \leqslant 400$. This observation was well supported by three-dimensional simulations additionally carried out using *LESOCC*. The results of the two-dimensional and three-dimensional computations are commensurate with the experiments of Armaly et al. [11].

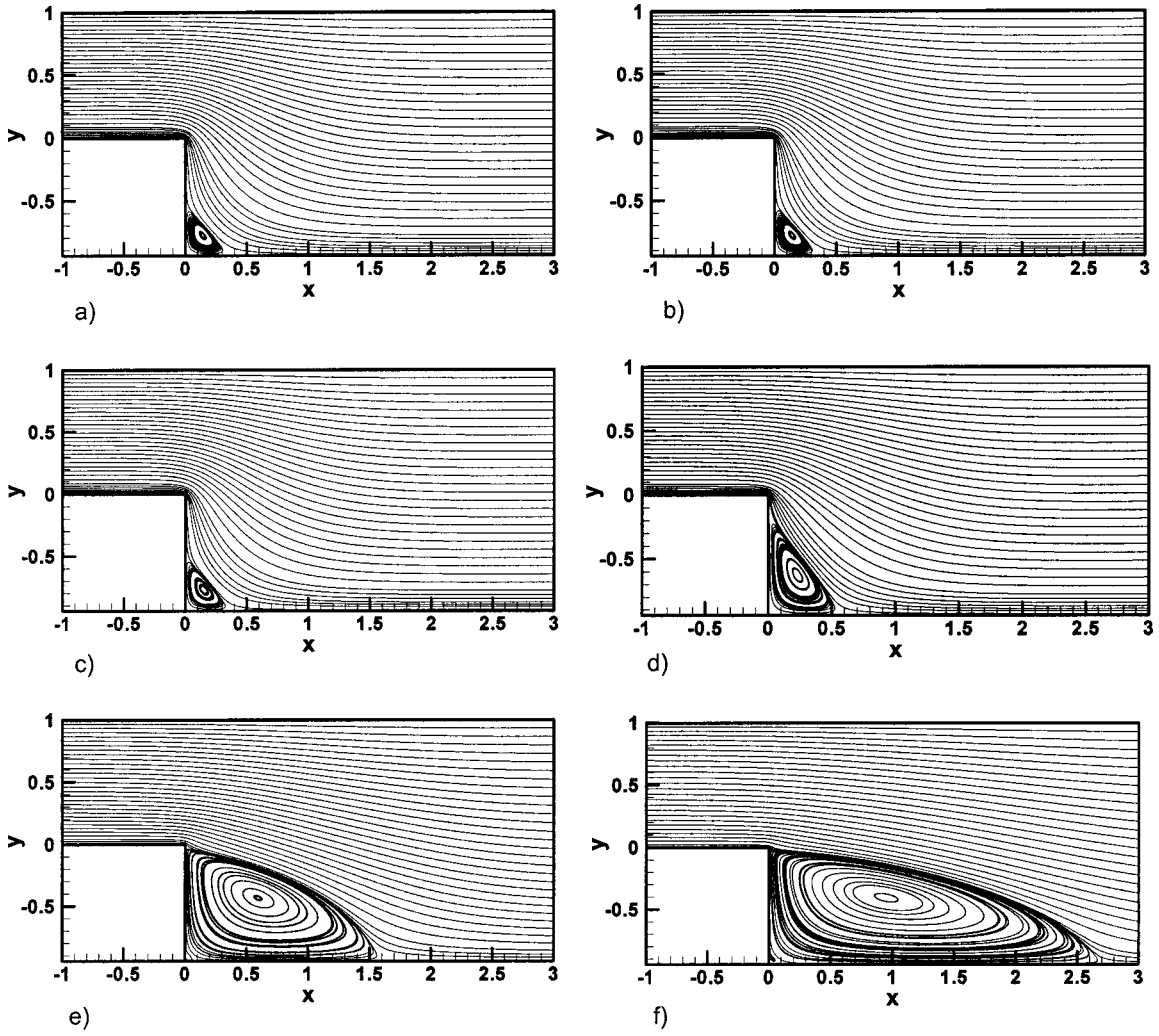

Fig. 3 Flow in the vicinity of the step. Expansion ratio $H/h=1.9423$; $10^{-4}\leq Re_D\leq 10^2$. (a) $Re_D=0.0001$; (b) $Re_D=0.1$; (c) $Re_D=1$; (d) $Re_D=10$; (e) $Re_D=50$; (f) $Re_D=100$.

In Fig. 3(*a*)–(*c*), the streamline patterns for $\mathrm{Re}_D=10^{-4}$, 10^{-1} and 1 are depicted. In all three cases shown, the flow follows the upper convex corner without revealing a flow separation. Furthermore, a corner vortex is found in the concave corner behind the step. In this range of very small Reynolds numbers ($10^{-4}\leq \mathrm{Re}_D \leq 1$), the size of this vortical structure is nearly constant varying between $x_1/h=0.350$ (for $\mathrm{Re}_D=10^{-4}$) and 0.365 (for $\mathrm{Re}_D=1$). Under these conditions, the effect of inertia forces can be assumed to be negligible compared with viscous forces often denoted as molecular transport. Hence the flow resembles the Stokes flow.

For a detailed analysis, the governing equations for the general case of Navier-Stokes flow given by Eqs. (1) and (2) are rewritten in a streamfunction-vorticity formulation eliminating the pressure:

$$\frac{\partial \psi}{\partial y}\frac{\partial \omega}{\partial x}-\frac{\partial \psi}{\partial x}\frac{\partial \omega}{\partial y}=\frac{1}{\mathrm{Re}_D}\nabla^2\omega \tag{5}$$

with

$$u=\frac{\partial \psi}{\partial y},\quad v=\frac{\partial \psi}{\partial x}\quad \text{and}\quad \omega=\frac{\partial u}{\partial y}-\frac{\partial v}{\partial x}. \tag{6}$$

The stream function ψ and the vorticity ω are related by

$$\omega=\nabla^2\psi. \tag{7}$$

For the description of creeping motion ($\mathrm{Re}_D\rightarrow 0$), the vorticity transport equation (5) reduces to the right-hand side of this equation, which in combination with Eq. (7) yields a biharmonic equation for the stream function ψ:

$$\nabla^4\psi=0. \tag{8}$$

This can be solved subject to appropriate boundary conditions. Based on analytical work, Moffatt [2] derived an expression for the complex stream function for the flow in the vicinity of sharp corners. In polar coordinates (r,θ) with the origin in the corner, the solution reads

$$\psi(r,\theta)=Kr^{\lambda}[\cos((\lambda-2)\alpha)\cos(\lambda\theta)-\cos(\lambda\alpha)\cos((\lambda-2)\theta)]. \tag{9}$$

The complex coefficient K is determined by the nature of the far-field flow. The complex exponent λ satisfies the nonlinear algebraic equation

$$\lambda\tan(\lambda\alpha)=(\lambda-2)\tan(\lambda-2)\alpha \tag{10}$$

where 2α defines the angle between two rigid boundaries. Under the condition $2\alpha<146$ deg Moffatt [2] showed the existence of an infinite sequence of closed eddies with decreasing size and strength in the sharp corner (see Fig. 1) now known as Moffatt eddies. Moffatt also demonstrated that even for finite Reynolds

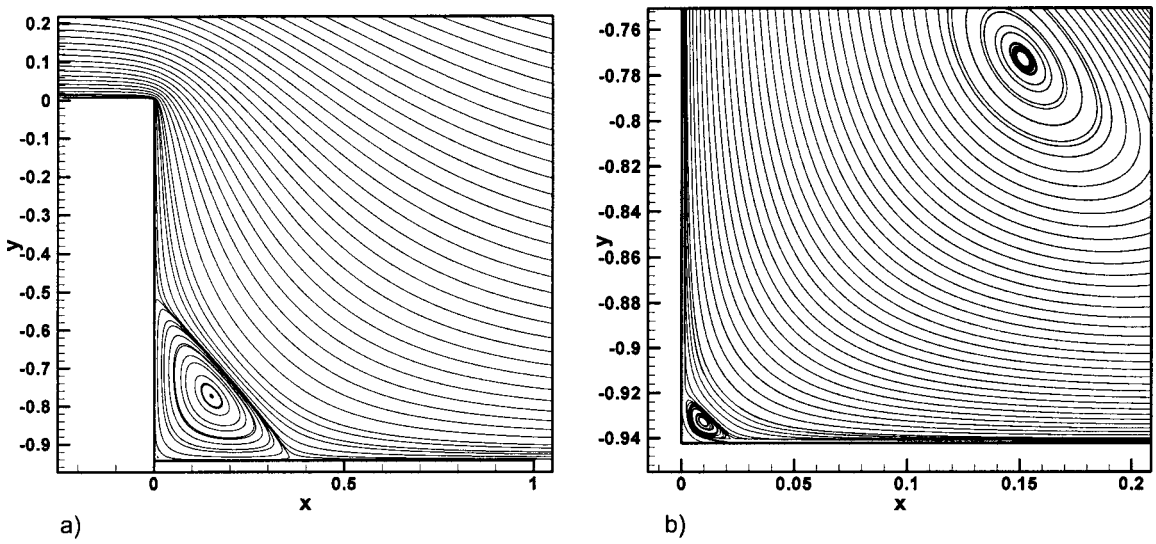

Fig. 4 Flow in the vicinity of the step. Expansion ratio $H/h=1.9423$; $Re_D=1$. (a) Zoom of the concave corner showing the first Moffatt eddy; (b) Increased zoom showing additionally the second Moffatt eddy.

numbers, the flow in the direct vicinity of the corner can still be described by the creeping flow assumption. It is therefore interesting to investigate whether for a finite Reynolds number, Moffatt vortices exist in the backward-facing step flow and whether they can be predicted by numerical solutions of the Navier-Stokes equations. Exemplarily the case of $\mathrm{Re}_D=1$ was chosen. At the upper convex corner of the step, $2\alpha=270$ deg and hence far beyond the critical value. In coincidence with the theory, no Moffatt eddy is found in the prediction. However, much more interesting is the lower concave corner with $2\alpha=90$ deg, where the condition on α for the existence of Moffatt eddies is satisfied.

Trying to capture the corner eddies numerically, a refined simulation applying the local grid refinement technique was carried out. The resolution in either direction near the corner point was taken as $\Delta x_{\min}/h=\Delta y_{\min}/h=0.001$. The entire domain was divided into seven different blocks and in total 310,784 control volumes were employed. Figure 4(*a*) depicts the streamlines in the vicinity of the corner showing the first corner vortex. Additionally, Fig. 4(*b*) shows a increased zoom of the corner region revealing that the second corner eddy (Moffatt eddy) could be resolved at the finite Reynolds number $\mathrm{Re}_D=1$. Based on Moffatt's considerations, an infinite sequence of eddies has to be expected but with reasonable resources it was not possible to resolve the third and subsequent eddies. This is due to the fact that the dimensions of successive eddies fall off in geometric progression with a ratio of $r_n/r_{n+1}=\exp(2.79)\approx 16.28$ for the α-value considered (Moffatt [2]). Here r_n and r_{n+1} are the distances of the center of the nth and $(n+1)$th eddy from the corner, respectively. The ratio of sizes of the first and second eddies found in the prediction are in close agreement with the theoretical value mentioned above. Moffatt also derived a measure for the intensity of consecutive eddies showing a fall-off with a geometric progression similar to the size. However, for a right-angle $(2\alpha=90)$ deg the eddy intensity drops more rapidly than the size at a ratio of $\exp(7.63)\approx 2059$. These considerations explain why the resolution of more than two corner vortices is extremely costly and hence was not taken into account.

Moffatt [2] noted in his paper that the size of the first corner vortex for $\mathrm{Re}_D\to 0$ is determined by conditions far from the corner where driving forces agitate the fluid. For the backward-facing step flow two important parameters are obviously responsible for the far-field flow. The first is given by the geometrical configuration, which can be defined by the expansion ratio h/H. The second is the Reynolds number. Figure 3 clearly demonstrates the effect of the Reynolds number for a fixed expansion ratio $H/h=1.9423$. As mentioned above, the size of the first eddy is nearly constant for all Reynolds numbers below $\mathrm{Re}_D=1$. This is also depicted in Fig. 5, showing the length x_1 of the first corner eddy behind the step (recirculation region) normalized by the step height S as a function of Re_D. However, for $\mathrm{Re}_D>1$ the corner vortex strongly increases in size. As a direct consequence, the corner vortex reaches up to the corner of the step at $\mathrm{Re}_D\approx 10$ and covers the complete face of the step. Hence a change in the entire flow structure is observed and the notation of a *corner vortex* has to be replaced by the notation *recirculation region*, which for $\mathrm{Re}_D>10$ better reflects the flow structure. With increasing Reynolds number the size of the recirculation region steadily increases.

In Fig. 6, streamline patterns for four different Reynolds numbers ($\mathrm{Re}_D=200$, 400, 600 and 800) are displayed, showing the increasing size of the recirculation region behind the step up to about $x_1/S\approx 12$ at $\mathrm{Re}_D=800$. Figure 7 shows the variation of reattachment length as a function of the Reynolds number. The agreement of the present predictions and the experimental results of Armaly et al. [11] for the vertical mid-plane ($z=W/2$) is excellent for $\mathrm{Re}_D\leqslant 400$. However, for $\mathrm{Re}_D\geqslant 400$ a discrepancy between computations and measurements at $z=W/2$ is visible,

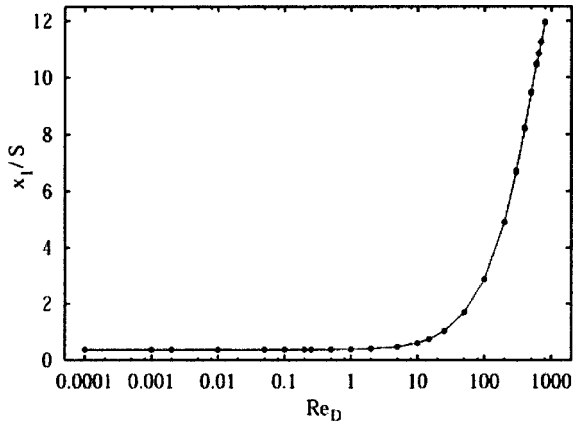

Fig. 5 Length x_1 of the first corner eddy behind the backward-facing step (expansion ratio $H/h=1.9423$) normalized by the step height S.

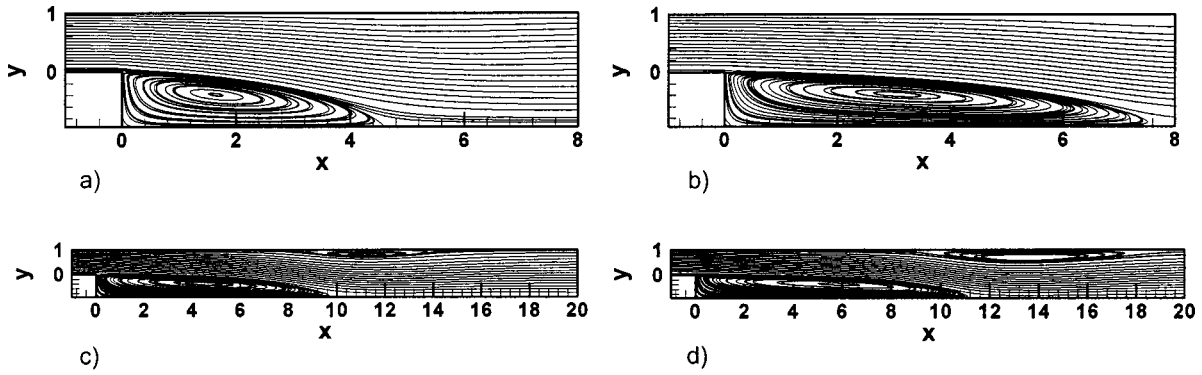

Fig. 6 Flow in the vicinity of the step. Expansion ratio $H/h=1.9423$; $200 \leq Re_D \leq 800$; two-dimensional simulations; (a) $Re_D=200$; (b) $Re_D=400$; (c) $Re_D=600$; (d) $Re_D=800$.

which obviously increases with Re_D. In order to improve these predictions, a variety of computations with different domain sizes, different resolutions and flow solvers (*FASTEST-2D* and *LESOCC*) were carried out. However, even on the finest grid and with an extremely long computational domain, the deviations observed between the measurements of Armaly et al. [11] and the present simulations could not be reduced. As expected from previous predictions by Armaly et al. and others (e.g. Kim and Moin [13]), which, however, used much coarser grid resolutions, the deviations mentioned above have to be attributed to the restriction to two-dimensional flow in the computations.

In addition to the primary recirculation zone, there exists a secondary recirculation zone near the upper wall for $Re_D>400$. The adverse pressure gradient due to the sudden expansion at the edge of the step induces this separated flow. In Figs. 6(*c*) and (*d*), the secondary recirculation region is clearly visible for $Re_D=600$ and 800, respectively. Figure 8 shows the starting position of the secondary recirculation zone (x_4/S) and the corresponding end (x_5/S) as a function of the Reynolds number. The size of the secondary recirculation zone increases with increasing Reynolds number while at the same time the flow structure is moving in a streamwise direction. Far downstream of the step, the flow recovers to a parabolic profile. However, at high Reynolds numbers such as $Re_D=800$, the flow recovery takes more than 20 step heights.

Figure 9 describes the variation of the primary reattachment lengths with Reynolds numbers for different expansion ratios, namely 1.9423, 2.5 and 3. At Reynolds numbers smaller than 400 the flow was predominantly two-dimensional. The reattachment lengths (x_1/h) increase with increase in the expansion ratio; for example, at a Reynolds number of 400, the reattachment lengths are 7.708, 10.214 and 12.409 for the expansion ratios of 1.9423, 2.5 and 3, respectively. The two-dimensional flow becomes unsteady with increasing Reynolds numbers. For an expansion ratio $H/h=1.9423$ the steady character of the two-dimensional backward-facing step flow was revealed over the entire Reynolds number range ($Re_D \leq 800$) investigated. For the case of expansion ratio $H/h=3$, the unsteadiness was observed at a Reynolds number of 500. The flow field demonstrated a low frequency oscillation at this Reynolds number.

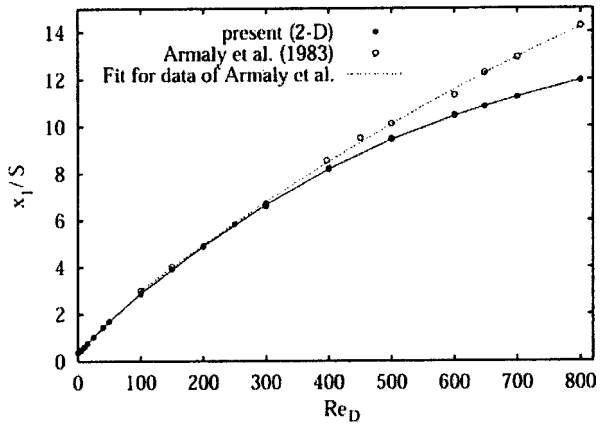

Fig. 7 Length x_1 of the primary recirculation region behind the backward-facing step (expansion ratio $H/h=1.9423$) normalized by the step height S

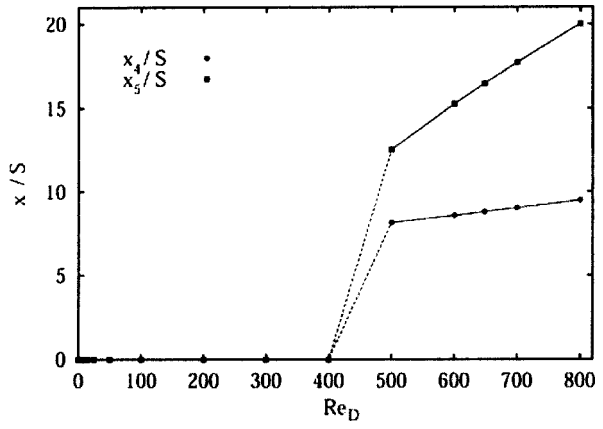

Fig. 8 Length x_4 and x_5 of the secondary recirculation region (on the roof) behind the backward-facing step (expansion ratio $H/h=1.9423$) n ormalized by the tep height S

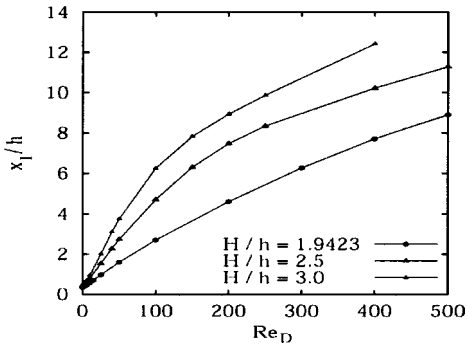

Fig. 9 Length of the primary recirculation region behind the backward-facing step x_1 for different expansion ratios, $H/h=1.9423$, 2.5, and 3.0

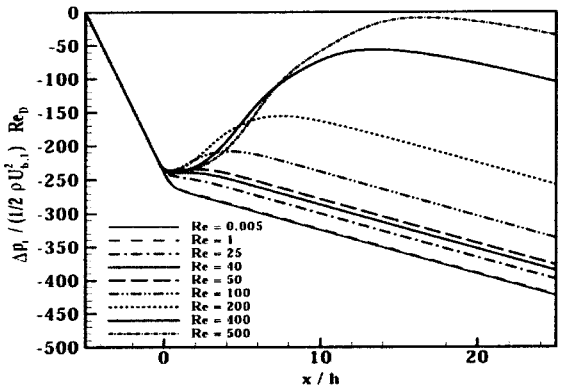

Fig. 10 Dimensionless pressure loss $\Delta p_t/(0.5\rho U_{b,1}^2)\cdot Re_D$ in the streamwise direction of the channel. Expansion ratio H/h=1.9423; Reynolds number range $5\cdot 10^{-3}\leqslant Re=Re_D\leqslant 5\cdot 10^2$.

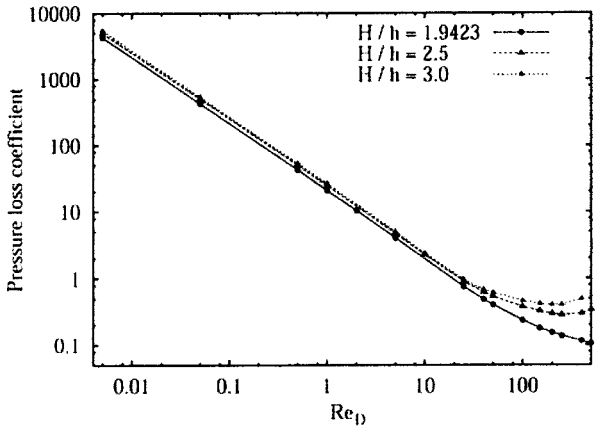

Fig. 11 Pressure loss coefficient ξ in the channel for different Reynolds numbers Re_D and expansion ratios H/h

4.1.2 Pressure Losses. An important engineering quantity for the design of channel systems with varying cross-sections is the pressure drop, which defines the performance of pumps required. For that purpose, the pressure drop in the backward-facing step geometry was evaluated for the expansion ratios and Reynolds numbers of interest in this study. Based on the two-dimensional simulations, the total pressure drops $\Delta p_t/(0.5\rho U_{b,1}^2)$ occurring on the axis of the channel are shown as a function of the Reynolds number in Fig. 10 for an expansion ratio $H/h=1.9423$. The pressure distributions for the Reynolds numbers range $0.005\leqslant \mathrm{Re}_D\leqslant 25$ are basically linear combinations of the pressure drops in the channels before and after the step, denoted Δp_1 and Δp_2, respectively. For a fully developed laminar channel flow, this irreversible pressure drop related to friction can be analytically determined as

$$\Delta p_1=\frac{\lambda}{\mathrm{Re}_D}\frac{L_u}{h}\frac{\rho}{2}U_{b,1}^2 \quad \text{and} \quad \Delta p_2=\frac{\lambda}{\mathrm{Re}_D}\frac{L_d}{H}\frac{\rho}{2}U_{b,2}^2, \tag{11}$$

where L_u and h are the length and height of the channel upstream of the step and L_d and H denote the length and height downstream of the step, as sketched in Fig. 2. The quantities $U_{b,1}$ and $U_{b,2}=U_{b,1}h/H$ describe the bulk (mean) velocities in either part of the channel. Based on the present definition of the Reynolds number [see Eq. (4)], the friction coefficient for the channel is $\lambda=48$. With regard to Eq. (11), the following aspects should be mentioned. First, it is obvious why for highly viscous flows (i.e. low Re_D) the pressure decreases linearly in streamwise direction showing different slopes in both parts of the channel. Additionally, it is clear why the dimensionless pressure drop in Fig. 10 was scaled with the Reynolds number Re_D leading to matching curves in the upstream channel over the entire Reynolds number range. If no other losses or gains are of importance, the pressure distributions are linear combinations of the pressure drops Δp_1 and Δp_2 as mentioned for $0.005\leqslant \mathrm{Re}_D\leqslant 25$.

However, this trend of streamwise pressure variation differs for $\mathrm{Re}_D>40$. In addition to the irreversible pressure drop discussed above, a reversible pressure rise near the step has to be taken into account because its relative importance increased. This pressure rise corresponds to the Bernoulli effect, associated with the decrease in mean velocity due to the sudden expansion:

$$\Delta p_{\exp}=\frac{\rho}{2}(U_{b,1}^2-U_{b,2}^2)=\frac{\rho}{2}U_{b,1}^2\left(1-\frac{h^2}{H^2}\right) \tag{12}$$

Hence the dimensionless pressure rise at the expansion $\Delta p_{\exp}/(0.5\rho U_{b,1}^2)$ is solely a function of the expansion ratio corresponding to the Bernoulli effect due to changes in the flow area. Owing to the special scaling in Fig. 10, the product increases with increasing Reynolds number. After reaching the peak, the streamwise pressure distribution in the channel follows again the same slope for all Reynolds numbers. Consequently, the total pressure drop in a backward-facing step geometry can be decomposed into

$$\Delta p_t=\Delta p_1+\Delta p_2-\Delta p_{\exp}+\xi\left(\frac{\rho}{2}U_{b,1}^2\right) \tag{13}$$

The last term in Eq. (13) takes into account the irreversible pressure drop occurring due to additional losses at the step. In contrast to Eq. (11) given for fully developed channel flow, a slightly modified formulation of Δp_2 is reasonable for the cases where a recirculation region is found behind the step:

$$\Delta p_2=\frac{\lambda}{\mathrm{Re}_D}\frac{(L_d-x_1)}{H}\frac{\rho}{2}U_{b,2}^2=\frac{\lambda}{\mathrm{Re}_D}\frac{(L_d-x_1)}{h}\left(\frac{h}{H}\right)^3\frac{\rho}{2}U_{b,1}^2, \tag{14}$$

where x_1 denotes the primary reattachment length determined as a function of Re_D and H/h in Fig. 9. Based on the determination of Δp_t by the predictions, the coefficient of irreversible pressure drop ξ was evaluated for various Reynolds number and expansion ratios. The results are shown on a double-logarithmic scale in Fig. 11. The value of ξ decreases with increasing Reynolds number. Higher expansion ratios produce higher coefficients of the irreversible pressure drop ξ, as expected.

4.2 Three-Dimensional Predictions: Flow Field. At relatively low Reynolds numbers ($\mathrm{Re}_D\leqslant 400$), the mid-plane flow field in a channel with an expansion ratio $H/h=1.9423$ is accurately predicted by two-dimensional simulations. Beyond a Reynolds number of about 400, the side wall influences the structure of the laminar flow behind the step. The measured reattachment lengths at the mid-plane and the predictions of two-dimensional simulations do not match. The discrepancies between the experimental result and the two-dimensional simulation are the consequence of the three-dimensionality that influences the flow structure at the mid-plane of the channel. In order to prove this, we compared the three-dimensional numerical simulation and the experimental results at three different Reynolds numbers, i.e., $\mathrm{Re}_D=397$, 648 and 800. The flow was found to be steady at these Reynolds numbers. Based on a nominally two-dimensional configuration assuming periodic boundary conditions in the spanwise direction, Kaiktsis et al. [16] observed an oscillatory behavior of the backward-facing step flow beyond $\mathrm{Re}_c\approx 700$. In the laboratory experiment of Armaly et al. [11] using a three-dimensional step geometry, the primary reattachment length exhibits a peak at $\mathrm{Re}_D\approx 1200$ followed by a subsequent decrease beyond this Reynolds number. This behavior can only be attributed to the action of the Reynolds stresses which must be present already for slightly

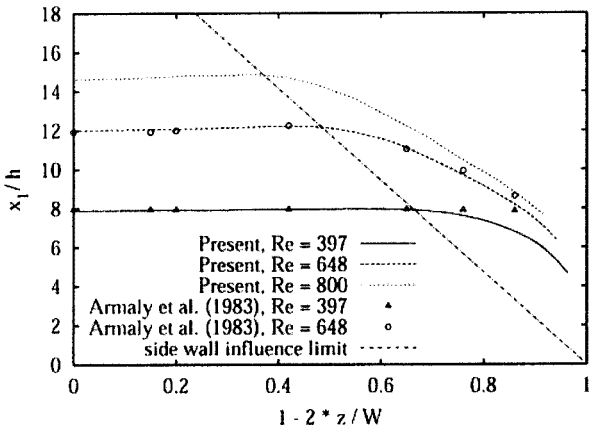

Fig. 12 Comparison of the spanwise location of the reattachment line past the backward-facing step at $Re=Re_D=397$, 648, and 800. Expansion ratio $H/h=1.9423$; aspect ratio $W/h=35$; present numerical 3-D simulation and experimental data of Armaly et al. [11].

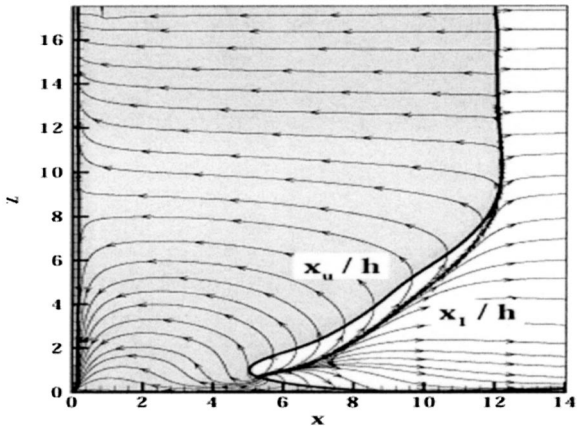

Fig. 14 Comparison between the boundary of the primary recirculation zone and the line of $\partial u/\partial y|_{wall}=0$. Flow past the backward-facing step at $Re_D=648$. Expansion ratio $H/h=1.9423$; aspect ratio $W/h=35$; (a) $y^*=0.046$; (b) $y^*=0.154$; (c) $y^*=0.273$; (d) $y^*=0.402$.

lower Reynolds numbers. This finding was complemented by our three-dimensional simulation at $Re_D=1300$. The unsteadiness of the flow was observed from the signals at different locations downstream of the expansion. In addition to the dominant frequency, f_1 another frequency, f_2, and the linear combination ($m_1 f_1 \pm m_2 f_2$, with integers m_1 and m_2) of f_1 and f_2 are present in the spectra. Hence in contrast to the observations of Kaiktsis et al. [16] for the two-dimensional configuration, the limit of steady flow in the three-dimensional case is expected to be at $Re_D \approx 1200$ characterized by the transitional regime ($1{,}200 < Re_D < 6{,}600$) found by Armaly et al. [11]. Consequently, the steady flow behavior predicted for $Re_D \leqslant 800$ is reasonable and in accordance with other simulations (e.g., Chiang and Sheu [22] and Williams and Baker [21]).

The comparison between the measured and predicted values of the primary reattachment lengths on the bottom wall (stepped wall) at $Re_D=397$ and 648, presented in Fig. 12, shows excellent agreement at different spanwise locations in the channel. For $Re_D=800$ no experimental data are provided by Armaly et al. [11]. Figure 12 also demonstrates the increasing side-wall effect with increasing Reynolds number. At $Re_D=397$ the influence of the side wall is visible up to about 36% of $W/2$, whereas about 54

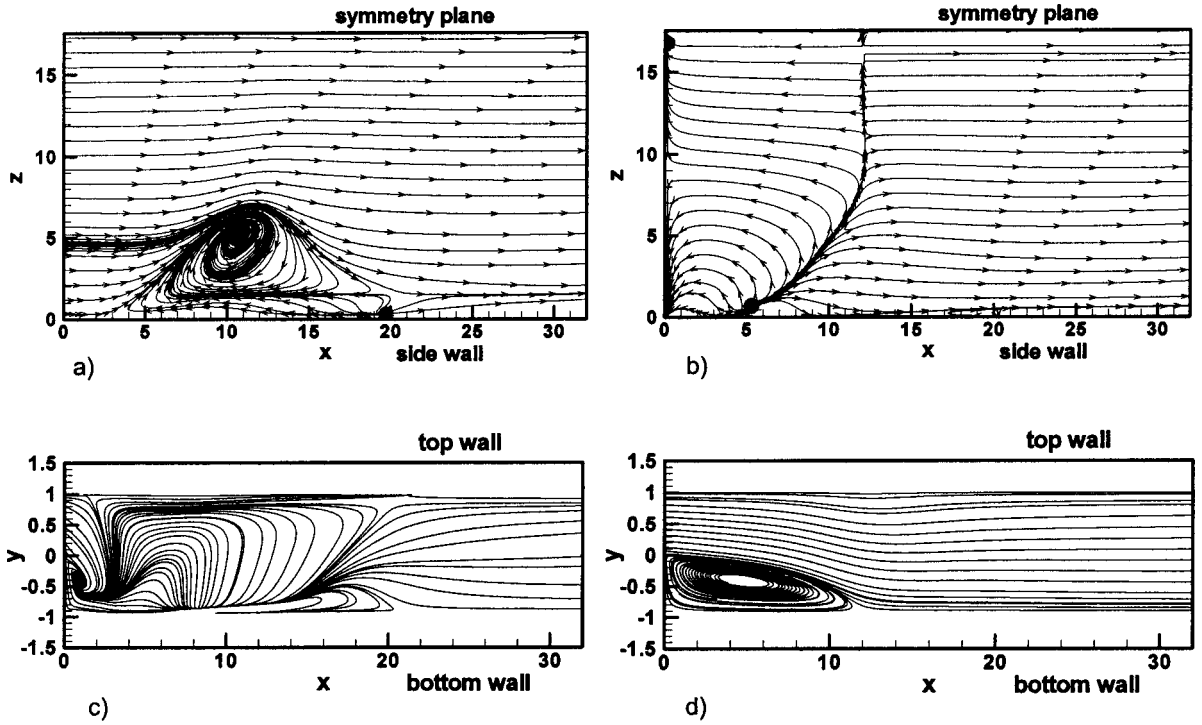

Fig. 13 Surface streamlines of the backward-facing step flow at $Re_D=648$. Expansion ratio $H/h=1.9423$; aspect ratio $W/h=35$; (a) Roof; (b) Bottom Wall; (c) Side Wall; (d) Symmetry Plane.

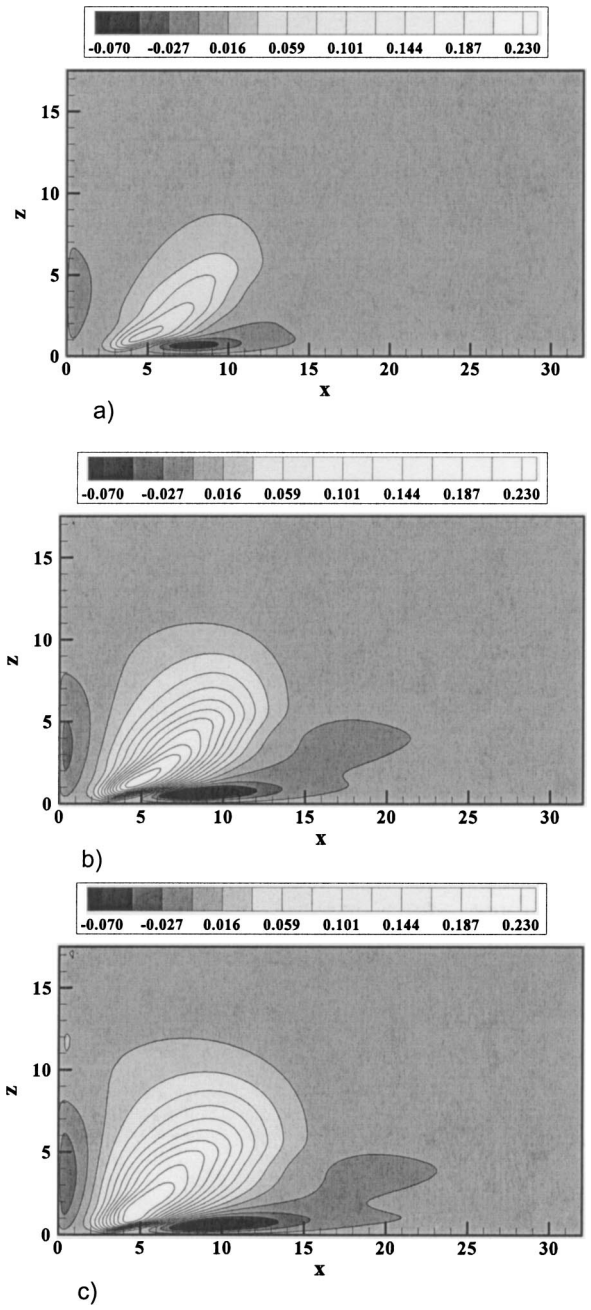

Fig. 15 Contours of the velocity component *w* on various *x-z* planes. *y denotes the dimensionless distance from the bottom wall; $H/h=1.9423$; $Re_D=648$**

and 66% are covered in case when $Re_D=648$ and 800, respectively. The results agree fairly well with predictions by Chiang and Sheu [22].

In order to understand the flow structure better, the limiting surface streamlines on the channel roof (Fig. 13(*a*)) and on the bottom (stepped) wall (Fig. 13(*b*)) are plotted at $Re_D=648$. The roof eddy extends about 40% of the width to the mid-plane. The limiting surface streamlines are the streamlines close to the surface (Hornung and Perry [38], Chiang and Sheu [22]). The kinematic aspects of the limiting surface streamlines are described by the singular points, namely nodes, saddle points and foci. The classification of critical points using local solutions of the Navier-Stokes equations was introduced by Oswatitsch [39]. The limiting streamlines diverge from the line of attachment. Usually this is known as positive streamsurface bifurcation. Figure 13(*b*) shows

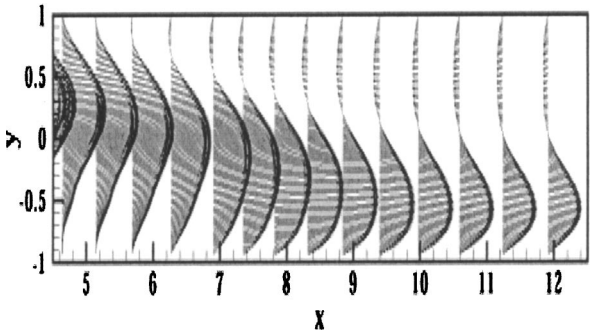

Fig. 16 Velocity vectors at a spanwise location of $z=1.05$; $H/h=1.9423$; $Re_D=648$

the diverging surface streamlines and the line of reattachment on the bottom wall for a Reynolds number of 648. Figures 13(*c*) and (*d*) depict the surface streamlines on the side wall and on the symmetric plane, respectively. The side wall shows the existence of a foci. All the surface streamlines spiral onto this point. The streamlines on the symmetric plane resembles with those of the two-dimensional simulation.

We have used the limiting streamlines to determine the boundary of the primary recirculation zone on the bottom wall (stepped wall) of the channel. As described by Chiang and Sheu [22], the surface streamlines tend to diverge from the line of attachment. The streamlines on both sides of this line of attachment move in opposite directions. Figure 14 shows that this boundary line (x_1/h) is different from the line (x_u/h) on which the gradient of the streamwise component of velocity at the wall $(\partial u/\partial y|_{wall})$ is zero. It is not incongruous to mention here that quantities such as x_1/h and x_u/h are identical for a two-dimensional flow. The effects of three-dimensionality culminate in the creation of a spanwise velocity component. This spanwise velocity component is responsible for the difference in the trajectory of the line that denotes the boundary of the primary recirculation region and the line on which $\partial u/\partial y|_{wall}$ is zero, particularly near the side wall. Moreover, it should be mentioned that these two lines are identical with each other over a span that extends a little more than about 50% of the half channel width in either direction of the symmetry plane. The discrepancies observed are more pronounced near the side wall where the *w* component of velocity is fairly strong. Another observation is that the reattachment length, based on the criterion of $\partial u/\partial y|_{wall}=0$ which defines a zero wall shear stress in the streamwise direction, increases near the side wall after attaining a minimum value. In fact, it reaches its maximum at the

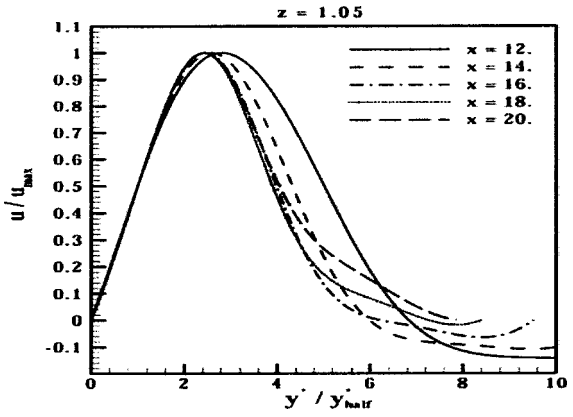

Fig. 17 Development of a wall jet in streamwise direction near the bottom wall. Spanwise location $z=1.05$; $H/h=1.9423$; $Re_D=648$; three-dimensional simulation.

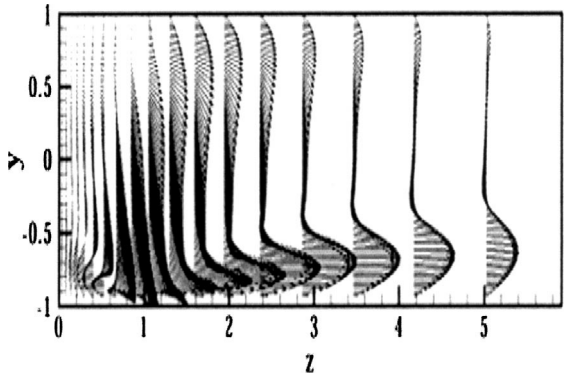

Fig. 18 Cross-stream velocity vectors at a streamwise location of $x=6$; $H/h=1.9423$; $Re_D=648$

side wall. The numerical data reveal this fact, even though it is not very evident from the figure. Our observation is well supported by Nie and Armaly [24].

The experiments of Armaly et al. [11] indicate that for an expansion ratio of 1.9423, the flow appears to be three-dimensional above $Re_D=400$. The transition to three-dimensionality is the primary source of discrepancies that appear in the comparison of two-dimensional computation and the experimental results above a Reynolds number of 400. In order to address the issues related to three-dimensionality, we resort to our three-dimensional simulation for $Re_D=648$. Figure 15 depicts the development of the spanwise component of velocity at four different horizontal planes located at $y^*=0.046$, 0.154, 0.273 and 0.402 from the bottom wall. Figures 15(*a*)–(*d*) show the gradual development of isolines of *w* velocity over different horizontal planes. The *w* velocity is initiated near the side wall, at the edge of the step as a consequence of development of a low-pressure zone and the fluid recirculation therein. The zone, influenced by the *w* velocity, grows larger as one moves in the perpendicular direction from the bottom wall. The maximum value of the *w* velocity is found to be 0.23.

The adverse pressure gradient due to the sudden expansion at the location of the step is responsible for the reverse flow together with the swirling motion in the spanwise direction, as shown by Williams and Baker [21]. They also showed the three-dimensional spiraling path from the side wall to the central symmetry plane. The swirling flow is responsible for the maximum and the minimum values that develop near the side wall in the spanwise distribution of the primary reattachment length (Fig. 12). The simulation for a Reynolds number of 648 shows a minimum around $(x=5;\ z=1)$. One noteworthy feature of the three-dimensional laminar flow is the shear layer that emanates adjacent to the step corner, impinges on the step wall and continues in the flow direction as a wall jet. Figure 16 shows the computed streamwise velocity profiles for a Reynolds number of 648 along the length of the channel at a spanwise location of $z=1.05$. After impingement, the flow continues downstream into the redeveloping flow region. A wall-jet-like characteristic feature is demonstrated during the redeveloping stage. The *u* velocity profile becomes self-similar in this regime. We investigate the *u* velocity profiles at a spanwise location of $z=1.05$ away from the side wall over the streamwise locations of $x=12$, 14, 16, 18 and 20. The *u* velocity profiles are normalized by $u_{\max}$, the local maximum value and the vertical distances from the bottom wall are normalized by y^*_{half}, the distance from the bottom wall to the location where the *u* velocity attains the value of local $u_{\max}/2$. Figure 17 illustrates the self-similar profiles at the lower part of the channel confirming the development of the wall-jet-like flow. The self-similarity holds good from the bottom wall until $y^*/y^*_{half}=3$. The maximum value of the *u* velocity profile at $x=12$ is 0.9867, whereas the maximum at $x=20$ is 0.6474.

Williams and Baker [21] found that yet another wall-jet-like profile forms at the step plane and grows in strength with increasing Reynolds number. They observed the presence of wall jet at the channel bottom wall, originated from the side wall and directed towards the channel mid-plane. The cross-stream velocity vectors (Fig. 18) at a streamwise distance of $x=6$ indicates that a wall-jet-like flow, in the spanwise direction, develops in the separating shear layer and moves towards the channel center. The formation of the wall jet in the spanwise direction is further demonstrated by our simulation at a Reynolds number of 648 in Figs.

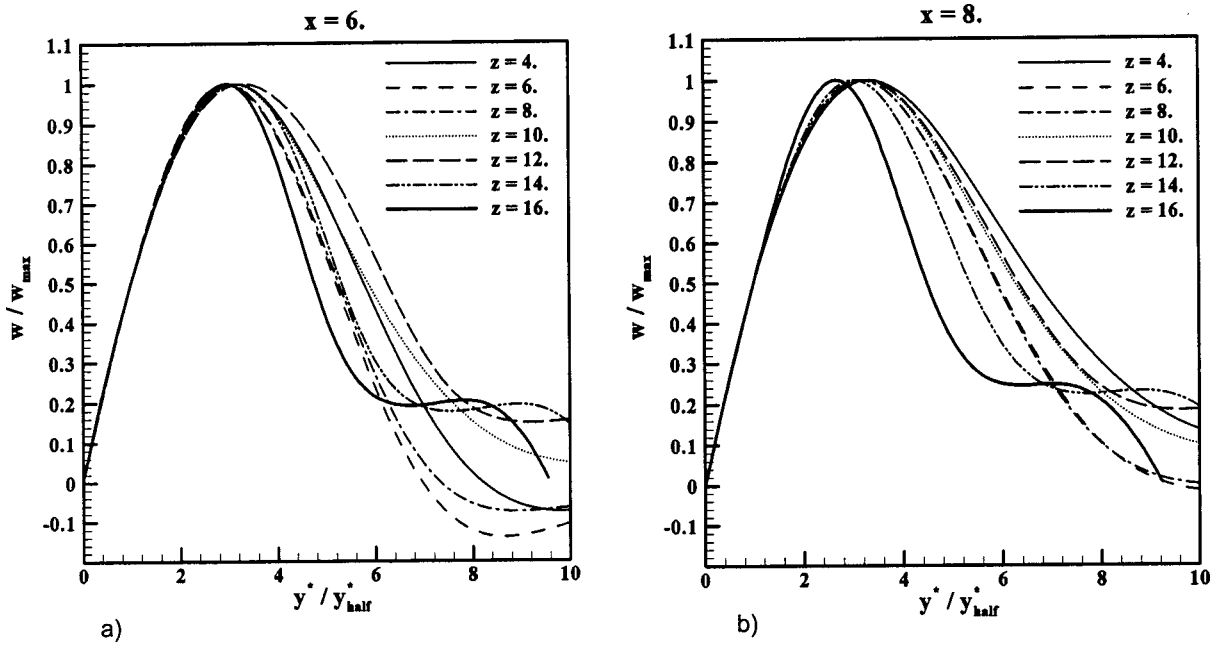

Fig. 19 Development of a wall jet in spanwise direction near the bottom wall. $H/h=1.9423$; $Re_D=648$. Steamwise locations: (a) $x=6$ (b) $x=8$.

19(*a*) and (*b*). The jet-like flow that develops in the spanwise direction is the culmination of the generation of the *w* velocity component from the side wall. The flow, predominantly the shear layer, emanates from the step edge and forms the separation zone at the sudden expansion. At about $x=5$, the flow impinges on the bottom wall, adjacent to the side wall and a jet-like flow emanates in the spanwise direction. The jet-like flow continues as a wall jet and interacts with the primary recirculation zone. We envisage the wall jet to exist at $x=6$ and 8. Figure 19(*a*) shows the self-similar wall-jet profile over various *z* locations at $x=6$. The *w* velocity distribution along *y* at a *z* location was normalized by $w_{\max}$, the maximum absolute value of the local *w* velocity distribution at that *z* location. The vertical distance from the bottom wall was expressed as y^* and this was normalized by y^*_{half}, the distance from the bottom wall to the point where the *w* velocity attains half of its maximum value. It is evident that the profiles at various *z* locations become self-similar in their bottom part, entailing the development of a wall jet up to the channel mid-plane. The deviation from a self-similar profile beyond $y^*/y^*_{half}=3.2$ can be explained by the difference in flow structure on the upper wall. Figure 19(*b*) reveals the same flow characteristics of the wall jets at various *z* locations at $x=8.0$. The value of $w_{\max}$ increases from 0.17 to 0.194 as one moves from $x=6$ to 8. However, a closer examination reveals that this maximum value of the *w* velocity decreases further downstream, say at $x=18$, and the wall-jet structure in the spanwise direction is no longer seen.

5 Conclusions

Laminar backward-facing step flow was investigated for a wide range of Reynolds numbers and expansion ratios by means of two- and three-dimensional simulations. The following conclusions can be drawn:

- For a wide range of Reynolds numbers, $10^{-4}\leqslant \mathrm{Re}_D\leqslant 1$, a corner vortex of nearly constant size is found in the concave corner behind the step. Based on the theory of Moffatt [2], an infinite sequence of closed eddies with decreasing size and strength is expected for $\mathrm{Re}_D\rightarrow 0$. In the present investigation, the first and second corner eddies were successfully predicted. Owing to the requirement for excessive computational resources, further eddies with decreasing strength could not be be captured with reasonable effort. Surprisingly, the phenomenon of creation of the Moffatt eddies (corner vortex) is not restricted to $\mathrm{Re}_D\rightarrow 0$ but is also evident at a finite Reynolds number of $\mathrm{Re}_D=1$.
- For the Reynolds number range $\mathrm{Re}_D\leqslant 400$ the flow past the backward-facing step can be predicted successfully by two-dimensional computations. The corner vortex observed for $\mathrm{Re}_D\leqslant 1$ reaches the step height at $\mathrm{Re}_D\approx 10$ (for $H/h=1.9423$) covering the entire face of the step. Hence the *corner vortex* steadily evolves into a *recirculation region* with increasing Re_D. Based on the two-dimensional predictions, excellent agreement with the experimental measurements of the flow field at the vertical mid-plane ($z=W/2$) is found for $\mathrm{Re}_D\leqslant 400$. As expected, this primary recirculation length increases non-linearly with increasing expansion ratio, H/h.
- As one of the most important engineering quantities for the design of a channel system, the pressure losses were evaluated for various expansion ratios and Reynolds numbers of interest in this study. The total pressure loss is subdivided into irreversible pressure drops related to friction in the channels before and after the step, the reversible pressure rise at the expansion and an irreversible pressure drop ξ occurring due to additional losses at the step. As expected, these losses increase with increasing step height *H* and decrease with increasing Reynolds number, except for $\mathrm{Re}_D>200$ and large expansion ratios, H/h.
- The three-dimensional predictions at three different Reynolds numbers ($\mathrm{Re}_D=397$, 648 and 800) were found to be in excellent agreement with the experimental results of Armaly et al. [11]. The effect of the side wall is evident for $\mathrm{Re}_D>400$, explaining the discrepancies observed between two-dimensional simulations and the experimental findings in the vertical mid-plane ($z=W/2$). In contrast to the observations of Kaiktsis et al. [16] an oscillatory behavior of the backward-facing step flow was found beyond $\mathrm{Re}_D\approx 1200$, which is in concurrence with the measurements of Armaly et al. [11].
- In the three-dimensional simulations it was observed that the boundary of the primary recirculation zone, determined by the surface streamlines on the bottom wall, is not identical with the line on which $\partial u/\partial y|_{wall}$ at the wall is zero.
- On the bottom wall, a wall jet in the streamwise direction with self-similar velocity profiles was identified as one of the main flow structures in the redeveloping region past the step. Furthermore, another wall jet in the spanwise direction, which is directed towards the channel mid-plane, was found near the bottom wall in the recirculation zone.

Acknowledgments

The stay of G. Biswas at LSTM Erlangen was supported by DAAD and KONWIHR (Competence Network on High-Performance Computing). The computations were carried out on the Fujitsu VPP 700 computer of the Leibniz Computing Center, Munich. This support is also gratefully acknowledged.

References

[1] Lee, Y. S. and Smith, L. C., 1986, *Analysis of power-law viscous materials using complex stream, potential and stress functions*, in Encyclopedia of Fluid Mechanics, vol. 1, Flow Phenomena and Measurement, ed. N. P. Cheremisinoff, pp. 1105–1154.
[2] Moffatt, H. K., 1964, *Viscous and resistive eddies near a sharp corner*, J. Fluid Mech., **18**, pp. 1–18.
[3] Roache, P. J., 1972, *Computational Fluid Dynamics*, Hermosa, New Mexico, pp. 139–173.
[4] Taylor, T. D., and Ndefo, E., 1971, *Computation of viscous flow in a channel by the method of splitting*, Proc. of the Second Int. Conf. on Num. Methods in Fluid Dynamics, Lecture Notes in Physics, vol. **8**, pp. 356–364, Springer Verlag, New York.
[5] Durst, F., and Peireira, J. C. F., 1988, *Time-dependent laminar backward-facing step flow in a two-dimensional duct*, ASME J. Fluids Eng., **110**, pp. 289–296.
[6] Alleborn, N., Nandakumar, K., Raszillier, H., and Durst, F., 1997, *Further contributions on the two-dimensional flow in a sudden expansion*, J. Fluid Mech., **330**, pp. 169–188.
[7] Brandt, A., Dendy, J. E., and Ruppel, H., 1980, *The multigrid method for semi-implicit hydrodynamic codes*, J. Comput. Phys., **34**, pp. 348–370.
[8] Hackbusch, W., 1985, *Multigrid Methods for Applications*, Springer, Berlin.
[9] Lange, C. F., Schäfer, M., and Durst, F., 2002, *Local block refinement with a multigrid flow solver*, Int. J. Numer. Methods Fluids **38**, pp. 21–41.
[10] Ladevéze, J., and Peyret, R., 1974, *Calcul numerique d'une solution avec singularité des equations de Navier-Stokes: écoulement dans un canal avec variation brusque de section*, J. Mech., **13**, no. 3, pp. 367–396.
[11] Armaly, B. F., Durst, F., Peireira, J. C. F., Schönung, B., 1983, *Experimental and theoretical investigation of backward-facing step flow*, J. Fluid Mech., **127**, pp. 473–496.
[12] Durst, F., and Peireira, J. C. F., and Tropea, C., 1993, *The plane symmetric sudden-expansion flow at low Reynolds numbers*, J. Fluid Mech., **248**, pp. 567–581.
[13] Kim, J., and Moin, P., 1985, *Application of a fractional-step method to incompressible Navier-Stokes equations*, J. Comput. Phys., **59**, pp. 308–323.
[14] Gartling, D. K., 1990, *A test problem for outflow boundary conditions—flow over a backward-facing step*, Int. J. Numer. Methods Fluids **11**, pp. 953–967.
[15] Lee, T., and Mateescu, D., 1998, *Experimental and numerical investigation of 2D backward-facing step flow*, J. Fluids Struct., **12**, pp. 703–716.
[16] Kaiktsis, L., Karniadakis, G. E., and Orszag, S. A., 1991, *Onset of three-dimensionality, equilibria, and early transition in flow over a backward-facing step*, J. Fluid Mech., **231**, pp. 501–528.
[17] Kaiktsis, L., Karniadakis, G. E., and Orszag, S. A., 1996, *Unsteadiness and convective instabilities in a two-dimensional flow over a backward-facing step*, J. Fluid Mech., **321**, pp. 157–187.
[18] Heenan, A. F., and Morrison, J. F., 1998, *Passive control of backstep flow*, Exp. Therm. Fluid Sci., **16**, pp. 122–132.
[19] Le, H., Moin, P., and Kim, J., 1997, *Direct numerical simulation of turbulent flow over a backward-facing step*, J. Fluid Mech., **330**, pp. 349–474.
[20] Kaltenbach, H.-J., and Janke, G., 2000, *Direct numerical simulation of flow separation behind a swept rearward-facing step at Re=3000*, Phys. Fluids, **12**(9), pp. 2320–2337.
[21] Williams, P. T., and Baker, A. J., 1997, *Numerical simulations of laminar flow over a 3D backward-facing step*, Int. J. Numer. Methods Fluids **24**, pp. 1159–1183.

[22] Chiang, T. P., and Sheu, T. W. H., 1999, *A numerical revisit of backward-facing step flow problem*, Phys. Fluids, **11**(4), pp. 862–874.
[23] Barkley, D., Gomes, M. G. M., and Henderson, R. D., 2002, *Three-dimensional instability in flow over a backward-facing step*, J. Fluid Mech., **473**, pp. 167–190.
[24] Nie, J. H., and Armaly, B. F., 2002, *Three-dimensional convective flow adjacent to backward-facing step—effects of step height*, Int. J. Heat Mass Transfer, **45**, pp. 2431–2438.
[25] White, F. M., 1991, *Viscous Fluid Flow*, 2nd ed., McGraw-Hill, New York.
[26] Orlanski, I., 1976, *A simple boundary condition for unbounded flows*, J. Comput. Phys., **21**, pp. 251–269.
[27] Breuer, M., and Rodi, W., 1996, *Large-eddy simulation of complex turbulent flows of practical interest*, In: Flow Simulation with High-Performance Computers II, ed. E. H. Hirschel, Notes on Numerical Fluid Mechanics, **52**, pp. 258–574, Vieweg Verlag, Braunschweig.
[28] Breuer, M., 1998, *Large-eddy simulation of the sub-critical flow past a circular cylinder: numerical and modeling aspects*, Int. J. Numer. Methods Fluids **28**, pp. 1281–1302.
[29] Breuer, M., 2002, *Direkte Numerische Simulation und Large-Eddy Simulation turbulenter Strömungen auf Hochleistungsrechnern*, Habilitationsschrift, Universität Erlangen-Nürnberg, Berichte aus der Strömungstechnik, ISBN 3-8265-9958-6, Shaker Verlag, Aachen.
[30] Demirdžić, I., and Perić, M., 1990, *Finite-volume method for prediction of fluid flow in arbitrary shaped domains with moving boundaries*, Int. J. Numer. Methods Fluids **10**, pp. 771–790.
[31] Patankar, S. V., and Spalding, D. B., 1972, *A calculation procedure for heat, mass and momentum transfer in three-dimensional parabolic flows*, Int. J. Heat Mass Transfer, **15**, pp. 1787–1806.
[32] Perić, M., Kessler, R., and Scheuerer, G., 1988, *Comparison of finite-volume numerical methods with staggered and colocated grids*, Comput. Fluids, **16**, pp. 389–403.
[33] Durst, F., and Schäfer, M., 1996, *A parallel blockstructured multigrid method for the prediction of incompressible flows*, Int. J. Numer. Methods Fluids **22**, pp. 549–565.
[34] Lange, C. F., Durst, F., and Breuer, M., 1998, *Momentum and heat transfer from cylinders in laminar flow at* $10^{-4} \leqslant Re \leqslant 200$, Int. J. Heat Mass Transfer, **41**, pp. 3409–3430.
[35] Lange, C. F., Durst, F., and Breuer, M., 1999, *Wall effects on heat losses from hot-wires*, Int. J. Heat Mass Transfer, **20**, pp. 34–47.
[36] Durst, F., Shi, J. M., and Breuer, M., 2002, *Numerical prediction of hot-wire corrections near walls*, J. Fluids Eng., **124**, pp. 241–250.
[37] Shi, J. M., Breuer, M., and Durst, F., 2002, *Wall effect on heat transfer from a micro cylinder in near-wall shear flow*, Int. J. Heat Mass Transfer, **45**, pp. 1309–1320.
[38] Hornung, H., and Perry, A. E., 1984, *Some aspects of three-dimensional separation, part I: streamsurface bifurcations*, Z. Flugwiss. Weltraumforsch., **8**(2), pp. 77–87.
[39] Oswatitsch, K., 1958, *Die Ablösungsbedingung von Grenzschichten*, In: Grenzschichtforschung, ed. H. Goertler, pp. 357–367, Springer Verlag Berlin/Göttingen/Heidelberg.